AIP | Applied Physics Letters

Si surface passivation by Al2O3 thin films deposited using a low thermal budget atomic layer deposition process

G. Seguini, E. Cianci, C. Wiemer, D. Saynova, J. A. M. van Roosmalen et al.

Citation: Appl. Phys. Lett. **102**, 131603 (2013); doi: 10.1063/1.4800541
View online: http://dx.doi.org/10.1063/1.4800541
View Table of Contents: http://apl.aip.org/resource/1/APPLAB/v102/i13
Published by the American Institute of Physics.

Si surface passivation by Al_2O_3 thin films deposited using a low thermal budget atomic layer deposition process

G. Seguini,[1,a)] E. Cianci,[1] C. Wiemer,[1] D. Saynova,[2] J. A. M. van Roosmalen,[2] and M. Perego[1,b)]
[1]*Laboratorio MDM, IMM-CNR, Via C. Olivetti 2, 20864 Agrate Brianza (MB), Italy*
[2]*ECN Solar Energy, Westerduinweg 3, NL-1755 ZG Petten, The Netherlands*

(Received 11 February 2013; accepted 25 March 2013; published online 5 April 2013)

High-quality surface passivation of crystalline Si is achieved using 10 nm thick Al_2O_3 films fabricated by thermal atomic layer deposition at 100 °C. After a 5 min post deposition annealing at 200 °C, the effective carrier lifetime is 1 ms, indicating a functional level of surface passivation. The interplay between the chemical and the field effect passivation is investigated monitoring the density of interface traps and the amount of fixed charges with conductance-voltage and capacitance-voltage techniques. The physical mechanisms underlying the surface passivation are described. The combination of low processing temperatures, thin layers, and good passivation properties facilitate a technology for low-temperature solar cells. © *2013 American Institute of Physics*. [http://dx.doi.org/10.1063/1.4800541]

Atomic layer deposition (ALD) of Al_2O_3 thin films has been demonstrated to be a valuable technique to grow high-quality surface passivation layers on crystalline Si (c-Si) for high-efficiency p- and n-type solar cells.[1–4] The passivation properties of Al_2O_3 can be rationalized invoking two independent physical effects: (i) chemical passivation of the interface defects that is determined by a significant reduction of the interface recombination centers and (ii) field-effect passivation, i.e., the reduction of the minority carrier concentrations at the c-Si/Al_2O_3 interface provided by an electrostatic shielding due to a built-in electric field within the oxide layer.[5–7] After thermal treatments, Al_2O_3 exhibits a high concentration of negative fixed charges ($Q_{ox} \approx 10^{12}$ cm^{-2}) and a low level of density of interface traps ($D_{IT} \approx 10^{11}$ eV^{-1} cm^{-2}).[8] Moreover, the relatively high Al_2O_3 band gap (≥6.2 eV) prevents any light absorption in the visible part of the solar spectrum, making this material particularly attractive for implementation at the sunny side of both p- and n-type solar cells.[3,9]

So far, the optimal combination of the process conditions for thermal ALD Al_2O_3 passivation layers has been set to a deposition temperature $T_{dep} \geq 200$ °C followed by a thermal treatment in N_2 at 400-450 °C for at least 10 min.[7,10] The plasma-enhanced ALD Al_2O_3, where the oxidation source is O_2 plasma, demonstrated a high level of surface passivation after anneal for 30 min at $T_{ann} = 425$ °C.[11] The effect was attributed to the higher Q_{ox} values. With respect to lower T_{ann} (≤350 °C), higher performances for thermal ALD compared to the plasma-enhanced ALD have been shown.[8,12] Although plasma-enhanced ALD is favorable for low temperature ALD process, other factors like interface exposure to oxygen radicals has to be considered as well due to the impact on the D_{IT} especially when lower temperature post deposition annealing processes are applied. Nevertheless, the experimental set-up for plasma ALD is significantly more complex than a conventional thermal ALD and this justifies the interest for a low temperature process using H_2O as oxygen precursor. The minimum Al_2O_3 thickness to maintain the combined effect of chemical and field effect passivation has been found to be 10 nm when using thermal ALD as a layer-deposition technique. Below 10 nm Al_2O_3 thickness, the passivation properties degrade due to the deterioration of the chemical passivation.[6,10,13] In order to enable a technology for low-temperature solar cell processing, it is essential to combine good surface passivation and low thermal budget of the thermal ALD Al_2O_3 layers.[14–16]

In this work, we focus on the possibility to achieve appropriate surface passivation by Al_2O_3 thin films deposited by thermal ALD at low temperature ($T_{dep} \leq 200$ °C). In addition, we apply a relatively short annealing time of 5 min at temperatures $T_{ann} \leq 350$ °C in N_2 atmosphere. In this way, the thermal budget during the sample preparation is significantly reduced, extending the relevance of this passivation approach to low temperature solar cell applications, e.g., crystalline Si-amorphous Si heterojunction solar cells, which have limited allowable annealing temperatures of about 200-250 °C.[15,16] We demonstrate that effective lifetime (τ_{eff}) values well above 1 ms can be achieved for 10-nm-thick Al_2O_3 films fabricated at $T_{dep} = 100$ °C and annealed at $T_{ann} = 200$-350 °C in N_2 atmosphere. The τ_{eff} results are correlated with extensive electrical characterization of the Al_2O_3 films to elucidate the intimate physical mechanisms that govern charge recombination at the c-Si/Al_2O_3 interface.

The 10-nm-thick Al_2O_3 films were obtained by thermal ALD using $Al(CH_3)_3$, trimethyl-aluminum (TMA), and H_2O as precursors at T_{dep} ranging between 100 °C and 200 °C. The TMA and H_2O exposure times were 0.015 s, the N_2 purge time following both reactant exposures was 8 s. The growth per cycle at 100 °C was 1.0 Å/cycle, increasing to 1.1 Å/cycle at 150-200 °C. After the ALD process, the films underwent a rapid thermal annealing (RTA) in N_2 for 5 min with T_{ann} ranging from 200 °C to 350 °C. Al_2O_3 films were deposited in a single process on both sides of H-terminated double-side polished p-type float zone FZ<100> Si wafers (resistivity 2-4 Ω cm, thickness 280 ± 25 μm). The τ_{eff} was measured by photo-conductance method. It is worth to notice that both sides of the sample were coated simultaneously

a)Electronic mail: gabriele.seguini@mdm.imm.cnr.it
b)Electronic mail: michele.perego@mdm.imm.cnr.it

which avoids any difference between the two c-Si/Al_2O_3 interfaces. Dedicated deposition processes on H-terminated single polished p- and n-type c-Si were performed to fabricate metal-oxide-semiconductor (MOS) test devices to evaluate the Q_{ox} and the D_{IT}. The H-terminated Si(100) surfaces were obtained by means of standard cleaning in a $HCl:H_2O_2:H_2O = 1:1:5$ solution for 10 min at 85 °C followed by a 30 s dip in diluted HF ($HF:H_2O = 1:50$) at room temperature.

The thickness and the structural properties of the films were measured by means of spectroscopic ellipsometry (SE) using an M2000-F (J.A. Woollam Co., Inc.) and by X-ray reflectivity (XRR) using a conventional laboratory Cu Kα X-ray source equipped with a parabolic multilayer monochromator and a position-sensitive detector. The functionality of the surface passivation using Al_2O_3 layers was monitored by τ_{eff} measurements as a function of the excess carrier density (Δn) using a WCT-120: Silicon Wafer Lifetime Tester from Sinton Instruments in transient or quasi-steady state mode.[17] The results are reported at $\Delta n = 10^{15}\,cm^{-3}$. Capacitance-voltage (CV) and conductance-voltage (GV) measurements were acquired simultaneously at 100 KHz in a dark environment in a shielded probe station at room temperature. The curves have been corrected for series resistances.[18] The metallization of the MOS structures were obtained by evaporating Al dots (0.08 mm^2 area) through a shadow mask on the front side. The ohmic contact on the back was fabricated by full evaporation with Al.

The thickness of the interfacial SiO_2 layer was reported to affect the passivation properties.[6,11,19] In our case, the combined measurements of the thickness by XRR and SE allow to conclude that the formation of an ultrathin interfacial layer (<0.7 nm) between Al_2O_3 and c-Si substrate is achieved after thermal treatment at 350 °C in N_2. These results are in perfect agreement with the systematic investigation made with transmission electron microscopy on similar samples where no recognizable interfacial layer was observed.[20] Moreover, also the time of flight secondary ion mass spectroscopy profiles [not shown] evidences the absence of an interlayer between the deposited films and the c-Si substrate either in the as-deposited sample or in the annealed ones. Presumably, the elevated reactivity of TMA during the early cycles of the deposition avoids the oxidation of the surface.

The passivation characteristics at the c-Si/Al_2O_3 interface were analyzed for the T_{dep} of 100, 150, and 200 °C and the T_{ann} between 200 and 350 °C. The results are reported in Fig. 1. In general, in our study, the thermal budget has a significant impact on the sample performance. In as-deposited state, τ_{eff} was a few tens of μs, recorded for $T_{dep} = 100$ °C. This parameter significantly improved after RTA in N_2 atmosphere. Even for the lowest $T_{ann} = 200$ °C in the series, τ_{eff} of 1 ms were detected for both $T_{dep} = 100$ °C and 150 °C. After annealing at $T_{ann} = 250$ °C, τ_{eff} was further increased. In case of $T_{dep} = 100$ °C, the passivation was even more improved after annealing at $T_{ann} = 350$ °C. As a result, the best τ_{eff} value of 1.3 ms was achieved. Furthermore, the samples deposited at $T_{dep} = 200$ °C showed τ_{eff} values in the lower edge for all applied annealing temperatures.

The effective lifetime values after anneal at 200-250 °C for deposition temperatures of 100 °C and 150 °C are comparable

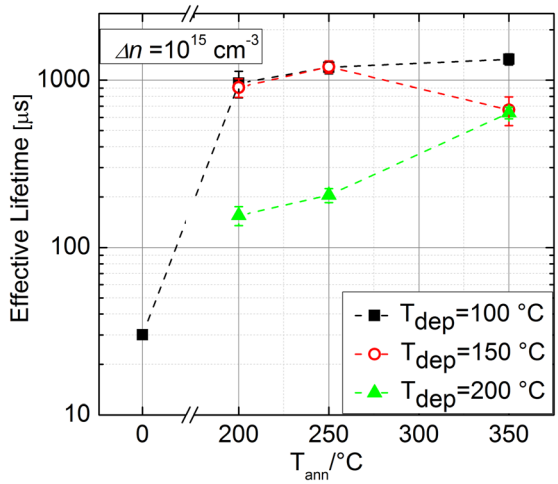

FIG. 1. Effective lifetime (τ_{eff}) measured at an injection level of $1 \times 10^{15}\,cm^{-3}$ of a 2-4 Ω cm p-type FZ wafer as a function of the annealing temperatures (T_{ann}) for different deposition temperatures (T_{dep}: 100 °C, 150 °C, and 200 °C). The lines are guide for the eye.

to the reports by other Authors for thermal ALD Al_2O_3 layers of thickness 10 nm applied for passivation of p-FZ wafers of [100] orientation in the resistivity range of 1.5–2.5 Ω cm.[10,12] It is worth to note that those data were obtained after annealing at high temperatures (T_{ann}>350 °C). In our case, the thermal load on the samples is significantly reduced compared to earlier studies both in terms of T_{dep} (200 °C was used) and T_{ann} (reports between 350 °C and 425 °C for 10–15 min). In as-deposited state, the effective lifetime was only a few tens of μs similar to other reports.[5]

In order to single out and understand the electrical properties behind the passivation mechanism, a detailed electrical characterization was performed in an extended range of deposition and annealing temperatures ($T_{dep} = 100$-200 °C, step 50 °C and $T_{ann} = 200$-350 °C, step 50 °C). Figure 2 depicts examples of typical CV curves for as-deposited samples at different T_{dep}. The position of the curves along the applied bias axis shows significant differences. The inversion/depletion transition region is positioned at negative voltages for $T_{dep} \leq 150$ °C and at positive voltages for $T_{dep} = 200$ °C. In the latter cases, marginal hysteresis effect appears as well.

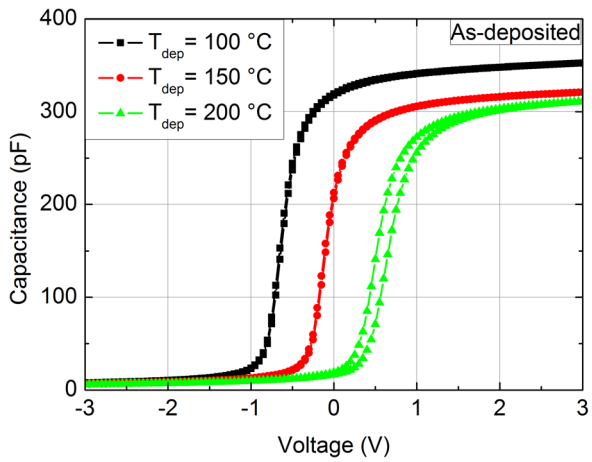

FIG. 2. 100 KHz CV curves for the as deposited samples at different deposition temperatures (T_{dep}: 100 °C, 150 °C, and 200 °C).

Nevertheless, the overall trends on Q_{ox} that we extracted are almost independent of this feature. The position of the flat band voltage (V_{FB}) allows the quantification of Q_{ox} that is the relevant parameter to monitor the field effect passivation.[21] The description of the evolution of the Q_{ox} for the various combinations of deposition and annealing conditions is reported in Fig. 3 as a function of the T_{ann} for the different T_{dep}. In the initial state, the film deposited at $T_{dep} = 100\,^{\circ}C$ exhibits a positive fixed charge, consistent with other reports,[22] that decreases in amount for $T_{dep} = 150\,^{\circ}C$ and becomes negative for $T_{dep} = 200\,^{\circ}C$. Following the effect of the thermal treatments, we can observe that the samples deposited at $T_{dep} = 200\,^{\circ}C$ are substantially unaffected by thermal treatments for $T_{ann} \leq 250\,^{\circ}C$. However, for samples deposited at $T_{dep} \leq 150\,^{\circ}C$, the thermal treatments at $T_{ann} \leq 250\,^{\circ}C$ are effectively modifying the Q_{ox} values. In particular, for $T_{dep} = 150\,^{\circ}C$, the thermal treatment changes the charge polarity at $T_{ann} = 250\,^{\circ}C$ while for the $T_{dep} = 100\,^{\circ}C$, the Q_{ox} starts changing at $T_{ann} = 200\,^{\circ}C$. For thermal treatments with $T_{ann} \geq 300\,^{\circ}C$, the samples deposited at $T_{dep} = 200\,^{\circ}C$ experienced only a little increase of the amount of the negative Q_{ox}. Differently, the samples deposited at $T_{dep} \leq 150\,^{\circ}C$ display a significant charge flip that results in a negative Q_{ox} of $(3 \pm 1) \times 10^{12}\,cm^{-2}$. This value is comparable to the high negative Q_{ox} values reported in the literature of $(4 \pm 1) \times 10^{12}\,cm^{-2}$ but as mentioned above the thermal load in our case is significantly lower.[10] The origin of the negative Q_{ox} has not been clearly identified yet and several interpretations are plausible: negatively charged traps like Al vacancies and/or O interstitials,[23,24] electron injection from Si through the interface may contribute to the negative charge associated with the trap states,[25] or the tetrahedral bonding configuration of the Al dominating at the interface.[26] More research is required to investigate the chemical and structural properties. The correlation of these properties with the electrical characteristics should help to identify which mechanism is responsible for the sign of Q_{ox} and, in particular, for the change of sign from positive to negative for the samples with $T_{dep} \leq 150\,^{\circ}C$ and $T_{ann} \geq 250\,^{\circ}C$.

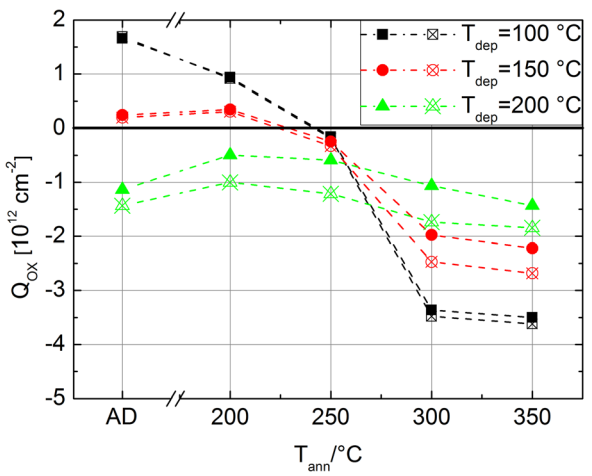

FIG. 3. Q_{ox} extracted from the V_{FB} values of the 100 KHz CV curves as a function of the annealing temperatures (T_{ann}) for different deposition temperatures (T_{dep}: 100 °C, 150 °C, and 200 °C).The values are reported for the two different sweep directions: from inversion to accumulation (solid symbols) and vice versa (open cross center symbols). The lines are guide for the eye. Error bars are comparable in size with the graph symbols.

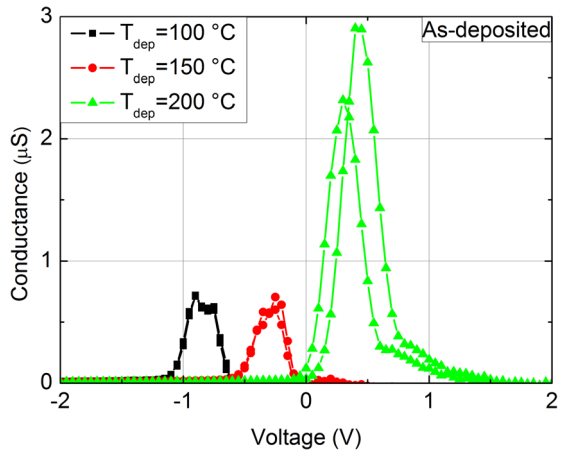

FIG. 4. 100 KHz GV curves for the as deposited samples at different deposition temperatures (T_{dep}: 100 °C, 150 °C, and 200 °C).

D_{IT} is the other relevant electrical property to get indications on the passivation behavior of the c-Si/Al_2O_3 interface since it is representative of the chemical passivation. In Fig. 4, the GV curves that were acquired simultaneously to the CV measurements depicted in Fig. 2 are reported. The position and the magnitude of the conductance peak highlight a clear difference between the samples deposited at $T_{dep} \leq 150\,^{\circ}C$ and the one at $T_{dep} = 200\,^{\circ}C$. This dependence on the T_{dep} exactly maps the one previously observed for the Q_{ox} trends in the CV curves. The evolution of the D_{IT} relative to the different combined process conditions (T_{dep} and T_{ann}) is reported in Fig. 5. The lowest D_{IT} values, below $3 \times 10^{10}\,eV^{-1}\,cm^{-2}$, are achieved for samples deposited at $T_{dep} \leq 150\,^{\circ}C$ and annealed at $T_{ann} \leq 250\,^{\circ}C$. The results show a significant improvement compared to the literature reports of $1 \times 10^{11}\,eV^{-1}\,cm^{-2}$ for 10 nm thermal ALD Al_2O_3 and demonstrate the passivation functionality of the current process.[10] On the other hand, the D_{IT} values rise to $\sim 1 \times 10^{11}\,eV^{-1}\,cm^{-2}$ when T_{dep} increases to 200 °C. For

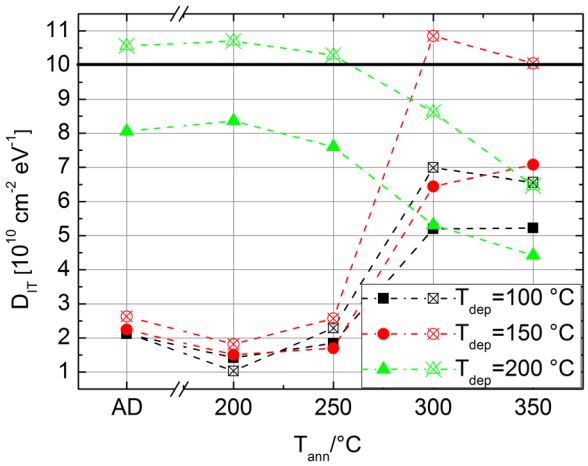

FIG. 5. D_{IT} extracted from the conductance peak position and magnitude values of the 100 KHz GV curves as a function of the annealing temperatures (T_{ann}) for different deposition temperatures (T_{dep}: 100 °C, 150 °C, and 200 °C). The values are reported for the two different sweep directions: from inversion to accumulation (solid symbols) and vice versa (open cross center symbols). The lines are guide for the eye. Error bars are comparable in size with the graph symbols.

$T_{ann} \geq 300\,^{\circ}C$, the samples show a different response to the effects of the thermal treatments. The results depend on the deposition temperature. For samples with $T_{dep} \leq 150\,^{\circ}C$, D_{IT} rises up when increasing annealing temperature while for the sample with $T_{dep} = 200\,^{\circ}C$ D_{IT} values decrease.

Two distinct ranges of deposition temperature ($T_{dep} \leq 150\,^{\circ}C$ and $T_{dep} = 200\,^{\circ}C$) are singled out in terms of D_{IT} and Q_{ox}, which are reported to be responsible for chemical passivation and field-effect passivation, respectively. GV analysis evidenced a very low D_{IT} value for ALD Al_2O_3 films as-deposited at $T_{dep} \leq 150\,^{\circ}C$, significantly increasing for $T_{dep} = 200\,^{\circ}C$. Correspondingly, positive Q_{ox} are present at the c-Si/Al_2O_3 interface for ALD Al_2O_3 films as-deposited at $T_{dep} \leq 150\,^{\circ}C$, while the polarity of Q_{ox} changes to negative at $T_{dep} = 200\,^{\circ}C$. The maximum negative Q_{ox} is measured to be above $Q_{ox} = 3.0 \times 10^{12}\,cm^{-2}$ for the $T_{dep} = 100\,^{\circ}C$ sample and $T_{ann} \geq 300\,^{\circ}C$. The minimum D_{IT} is measured to be below $3.0 \times 10^{10}\,eV^{-1}\,cm^{-2}$ for samples with $T_{dep} \leq 150\,^{\circ}C$ and $T_{ann} \leq 250\,^{\circ}C$. The electrical characteristics of the samples with $T_{dep} = 200\,^{\circ}C$ are less affected by the thermal treatments. These electrical characterizations identify $T_{dep} \leq 150\,^{\circ}C$ and $T_{ann} = 200\text{-}300\,^{\circ}C$ as the most promising conditions for the overall surface passivation.

The evolution of the τ_{eff} characteristics with the T_{ann} for the different T_{dep} needs detailed comments, because of the significant impact on the passivating properties of the Al_2O_3 layers. In particular, for the films of $T_{dep} = 200\,^{\circ}C$, the increase in T_{ann} from $200\,^{\circ}C$ to $350\,^{\circ}C$ improves the τ_{eff} from $\sim$150 to $\sim$650 μs. The τ_{eff} evolution can be understood following the variation of D_{IT} and Q_{ox}. The D_{IT} level improves for $T_{ann} = 350\,^{\circ}C$, $5.5 \times 10^{10}\,eV^{-1}\,cm^{-2}$ compared to $T_{ann} = 200\,^{\circ}C$, $\sim 1.0 \times 10^{11}\,eV^{-1}\,cm^{-2}$. Equally, the amount of negative Q_{ox} increases from $T_{ann} = 200\,^{\circ}C$, $-1.0 \times 10^{12}\,cm^{-2}$ to $T_{ann} = 350\,^{\circ}C$, $-2.0 \times 10^{12}\,cm^{-2}$. The behavior of the samples with $T_{dep} \leq 150\,^{\circ}C$ can be understood considering several aspects. The passivation becomes substantial upon annealing at $T_{ann} = 200\,^{\circ}C$, as demonstrated by τ_{eff} of 1 ms for both investigated deposition temperatures. This effect could be ascribed to the excellent level of chemical passivation due to the reduced D_{IT} below $2 \times 10^{10}\,eV^{-1}\,cm^{-2}$, irrespective of the low amount of positive Q_{ox}. When T_{ann} was increased to $350\,^{\circ}C$, the samples deposited at $T_{dep} = 100\,^{\circ}C$ improve the τ_{eff} characteristics even further. This effect indicates that the worsening of the D_{IT} is compensated by the improvement of the negative Q_{ox}. On the other hand, the samples deposited at $T_{dep} = 150\,^{\circ}C$ show τ_{eff} decrease at $T_{ann} = 350\,^{\circ}C$. The effect can be understood in terms of insufficient improvement of Q_{ox} to compensate for the D_{IT} degradation which is larger compared to the samples of $T_{dep} = 100\,^{\circ}C$.

The D_{IT} and the Q_{ox} contribute differently to the overall surface passivation. A low D_{IT} level corresponds to a limited number of recombination centers. In this condition, the electrostatic shielding of the interface for the minority carriers does not induce a further increase in the τ_{eff} value, since there is a limited amount of interface traps to be shielded. When the chemical passivation starts to decrease, the field effect passivation can become effective if there is a sufficient amount of Q_{ox} available. These results indicate three D_{IT} separate ranges: $D_{IT} < 3 \times 10^{10}\,eV^{-1}\,cm^{-2}$ yield excellent surface passivation for positive as well as negative Q_{ox} of $+9 \times 10^{11}\,cm^{-2}$ and $-2 \times 10^{11}\,cm^{-2}$, respectively. The sign and magnitude of Q_{ox} have no significant impact. The latter effect is consistent with the reports of good passivation of p- and n-type c-Si surfaces by both AlO_x and a-SiN_x:H layers which yield Q_{ox} of opposite polarity in the range of 1–6 $10^{12}\,cm^{-2}$. Low D_{IT} is also recognized as one of the prerequisites for functional low temperature solar cell technologies.[14–16] For D_{IT} between $3 \times 10^{10}\,eV^{-1}\,cm^{-2}$ and $7 \times 10^{10}\,eV^{-1}\,cm^{-2}$, the improvement in field effect passivation can compensate for the increase in D_{IT} and enable high effective lifetime values. Finally, for $D_{IT} > 8 \times 10^{10}\,eV^{-1}\,cm^{-2}$, the improvement in Q_{ox} is insufficient to ensure good passivation.

In conclusion, we show that the systematic mapping of the electrical properties of the c-Si/Al_2O_3 interface is a very powerful method in order to investigate the different contributions to the charge recombination at the c-Si/Al_2O_3 interface obtained by low temperature ALD process. The resulting data allow singling out an overall reduced thermal budget for suitable surface passivation. This is obtained by combining a low deposition temperature ($T_{dep} = 100\,^{\circ}C$) followed by annealing in N_2 at reduced temperature for short duration (T_{ann} of 200-350 °C, 5 min). Al_2O_3 layers of 10 nm thickness employing this adjusted thermal budget facilitate an optimal balance between D_{IT} and Q_{ox}. Consequently, good passivation of the c-Si interface is achieved as evidenced by τ_{eff} above 1 ms. The result makes these process conditions promising for low temperature solar cell applications.

This work was supported by the EU via project NanoPV (FP7-NMP3-SL-2011-246331). Mario Alia (MDM, IMM-CNR) and Esther Cobussen-Pool (ECN) are gratefully acknowledged for technical assistance. Sabina Spiga, Federico Ferrarese Lupi, Jacopo Frascaroli (MDM, IMM-CNR), and Arthur Weeber (ECN) are gratefully acknowledged for the fruitful discussions.

[1]J. Schmidt, A. Merkle, R. Brendel, B. Hoex, M. C. M. van de Sanden, and W. M. M. Kessels, Prog. Photovoltaics **16**, 461 (2008).
[2]S. Gatz, H. Hannebauer, R. Hesse, F. Werner, A. Schmidt, T. Dullweber, J. Schmidt, K. Bothe, and R. Brendel, Phys. Status Solidi (RRL) **5**, 147 (2011).
[3]J. Benick, B. Hoex, M. C. M. van de Sanden, W. M. M. Kessels, O. Schultz, and S. W. Glunz, Appl. Phys. Lett. **92**, 253504 (2008).
[4]R. Bock, S. Mau, J. Schmidt, and R. Brendel, Appl. Phys. Lett. **96**, 263507 (2010).
[5]B. Hoex, J. Schmidt, P. Pohl, M. C. M. van de Sanden, and W. M. M. Kessels, J. Appl. Phys. **104**, 044903 (2008).
[6]N. M. Terlinden, G. Dingemans, M. C. M. van de Sanden, and W. M. M. Kessels, Appl. Phys. Lett. **96**, 112101 (2010).
[7]G. Dingemans, M. C. M. van de Sanden, and W. M. M. Kessels, Electrochem. Solid-State Lett. **13**(3), H76–H79 (2010).
[8]G. Dingemans, N. M. Terlinden, D. Pierreux, H. B. Profijt, M. C. M. van de Sanden, and W. M. M. Kessels, Electrochem. Solid-State Lett. **14**(1), H1–H4 (2011).
[9]D. Zielke, J. H. Petermann, F. Werner, B. Veith, R. Brendel, and J. Schmidt, Phys. Status Solidi (RRL) **5**, 298 (2011).
[10]F. Werner, B. Veith, D. Zielke, L. Kühnemund, C. Tegenkamp, M. Seibt, R. Brendel, and J. Schmidt, J. Appl. Phys. **109**, 113701 (2011).
[11]B. Hoex, J. J. H. Gielis, M. C. M. van de Sanden, and W. M. M. Kessels, J. Appl. Phys. **104**, 113703 (2008).
[12]G. Dingemans, R. Seguin, P. Engelhart, M. C. M. van de Sanden, and M. M. Kessels, Phys. Status Solidi (RRL) **4**, 10 (2010).
[13]J. Frascaroli, G. Seguini, E. Cianci, D. Saynova, J. van Roosmalen, and M. Perego, Phys. Status Solidi A, **210**, 732 (2013).

[14]T. Mishima, M. Taguchi, H. Sakata, and E. Maruyama, Sol. Energy Mater. Sol. Cells **95**, 18 (2011).
[15]Q. Wang, Philos. Mag. **89**, 2587 (2009).
[16]W. van Sark, L. Korte, and F. Roca, *Physics and Technology of Amorphous-Crystalline Heterostructure Silicon Solar Cells* (Springer, 2012).
[17]R. A. Sinton and A. Cuevas, Appl. Phys. Lett. **69**, 2510 (1996).
[18]E. H. Nicollian and J. R. Brews, *Metal Oxide Semiconductor Physics and Technology* (Wiley, New York, 1982).
[19]J. J. H. Gielis, B. Hoex, M. C. M. van de Sanden, and W. M. M. Kessels, J. Appl. Phys. **104**, 073701 (2008).
[20]L. Lamagna, G. Scarel, and M. Fanciulli, J. Vac. Sci. Technol. A **27**, 443 (2009).
[21]D. K. Schroder, *Semiconductor Material and Device Characterization*, 3rd ed. (*John Wiley & Sons, Inc*., 2006).
[22]J. M. Rafi, M. Zabala, O. Beldarrain, and F. Campabadal, J. Electrochem Soc. **158**, G108 (2011).
[23]M. K. Matsunaga, T. Tanaka, T. Yamamoto, and Y. Ikuhara, Phys. Rev. B **68**, 085110 (2003).
[24]R. Weber, A. Janotti, and C. G. van de Walle, J. Appl. Phys. **109**, 033715 (2011).
[25]G. Dingemans, N. M. Terlinden, M. A. Verheijen, M. C. M. van de Sanden, and W. M. M. Kessels, J. Appl. Phys. **110**, 093715 (2011).
[26]K. Kimoto, Y. Matsui, T. Nabatame, T. Yasuda, T. Mizoguchi, I. Tanaka, and A. Toriumi, Appl. Phys. Lett. **83**, 4306 (2003).